applied sciences

MDPI

Article

Arbitrary Phase Modulation of General Transmittance Function of First-Order Optical Comb Filter with Ordered Sets of Quarter- and Half-Wave Plates

Jaehoon Jung [1] and Yong Wook Lee [2,3,*]

1 Department of Electronics and Electrical Engineering, Dankook University, Gyeonggi-do, Yongin 16890, Korea; andyjung@dku.edu
2 School of Electrical Engineering, Pukyong National University, Busan 48513, Korea
3 Industry 4.0 Convergence Bionics Engineering, Pukyong National University, Busan 48513, Korea
* Correspondence: yongwook@pknu.ac.kr; Tel.: +82-51-629-6323

Received: 17 July 2020; Accepted: 3 August 2020; Published: 6 August 2020

check for updates

Abstract: Here we theoretically and experimentally demonstrated the arbitrary phase modulation of a general transmittance function (GTF) of the first-order optical comb filter based on a polarization-diversity loop structure, which employed two ordered waveplate sets (OWS's) of a quarter-wave plate (QWP) and a half-wave plate (HWP). The proposed comb filter is composed of a polarization beam splitter (PBS), two equal-length polarization-maintaining fiber (PMF) segments, and two OWS's of a QWP and an HWP with each set located before each PMF segment. The second PMF segment is butt-coupled to one port of the PBS so that its principal axis should be 22.5° away from the horizontal axis of the PBS. First, we explained a scheme to find four waveplate orientation angles (WOA's) allowing the phase of a GTF to be arbitrarily modulated, using the way each component of the filter, such as a waveplate or PMF segment, affects its input or output polarization. Then, with the WOA finding method, we derived WOA sets of the four waveplates, which could give arbitrary phase retardations ϕ's from 0° to 360° to a GTF chosen here arbitrarily. Finally, we showed phase-modulated GTF's calculated at eight selected WOA sets allowing ϕ's to be 0°, 45°, 90°, 135°, 180°, 225°, 270°, and 315°, and then the predicted results were verified by experimentally measured results. It is concluded from the theoretical and experimental demonstrations that the GTF of our filter based on the OWS of a QWP and an HWP can be arbitrarily phase-modulated by properly controlling the WOA's of the four waveplates.

Keywords: optical filter; comb filter; polarization interference; general transmittance function; continuous phase modulation

1. Introduction

To date, optical comb filters have provided versatile spectrum controllability in the fields of interrogation of optical fiber sensors, wavelength routing in optical communications, and photonic processing of microwave signals [1–5]. In these comb filters, the capability of continuous wavelength tuning is a crucial function to pass desired spectral components or reject unwanted ones in optical signal processing. By utilizing a Mach-Zehnder interferometer structure [6,7], Sagnac birefringence loop structure [8,9], Lyot-type birefringence loop structure [10,11], and polarization-diversified loop structure (PDLS) [12–16], much effort has been exerted in implementing this continuous tunability of the absolute wavelength in comb filters. Among these filter configurations, optical comb filters based on a PDLS have superior flexibility in the wavelength switching or tuning of their output spectra [12–20]. Since 2017, successive works have been done to realize the continuous wavelength tuning of periodic transmission spectra in PDLS-based fiber comb filters [21–25]. A continuously wavelength-tunable PDLS-based zeroth-order comb filter containing one polarization-maintaining fiber (PMF) segment as a birefringent element (BE) was reported by employing three ordered waveplate sets (OWS's): an OWS of a half-wave plate (HWP) and a quarter-wave plate (QWP), another OWS of a QWP and an HWP, and two QWPs [21]. Apart from the zeroth-order comb filters, there have been several works reporting the implementation of the continuous wavelength tuning of flat-top [22,23], narrow [23,24], and arbitrary-shaped [25] passband transmission spectra, which could be obtained in a PDLS-based first-order comb filter having two PMF segments. In these previous studies on the first-order comb filters [22–25], only the OWS of an HWP and a QWP was adopted and placed before each PMF segment to continuously modulate the extra phase delay ϕ in the filter transmittance function. Another OWS of a QWP and an HWP may also be a candidate to achieve the ϕ modulation. To the best of our knowledge, the flexible wavelength tuning of arbitrary-shaped passband transmission spectra, that is, general transmittance functions (GTF's) in addition to some special transmittance functions such as transmittance functions with flattened and narrowed passbands, was not achieved by using an OWS of a QWP and an HWP. Arbitrary phase modulation of the GTF of the first-order comb filter leading to its flexible wavelength tuning should not be underestimated but rather rigorously explored, because application-specific spectral shapes are demanded in some spectral flattening filters and label erasers and their wavelength tuning capability can provide great efficiency to related optical systems. In particular, the new OWS will bring completely different sets of waveplate orientation angles (WOA's) where the phase ϕ of the filter transmittance function can be arbitrarily modulated. On top of that, the conventional scheme utilized to obtain WOA's theoretically in order to enable continuously tuning the filter wavelength [22–24], based on direct comparison between the filter transmittance function and the known analytic transmittance effortlessly found in literatures, is not suitable for finding theoretical WOA's for continuous frequency tuning of the GTF, because the exact mathematical expression of a desired GTF needed for specific applications is often difficult to seek. Here, we theoretically and experimentally demonstrated the arbitrary phase modulation of a GTF of the PDLS-based first-order fiber comb filter employing two OWS's of a QWP and an HWP. The proposed comb filter consists of a polarization beam splitter (PBS), two polarization-maintaining fiber (PMF) segments of equal length, and two OWS's of a QWP and an HWP with each OWS positioned before each PMF segment. The second PMF segment is butt-coupled to one port of the PBS so that its principal axis should be 22.5° away from the transverse-magnetic (TM) polarization axis of the PBS. Basically, polarization conditions, which should be satisfied to modulate the desired phase of a GTF, are explained by taking advantage of the spectral evolution of the input and output states of polarization (SOP's) of the second PMF in the narrowband transmittance function, on the basis of the continuous wavelength tuning mechanism of previously reported PDLS-based first-order narrowband comb filters [23,24]. Then, we explain a scheme to find four WOA's for the arbitrary phase modulation of a GTF, using how each component of the filter, such as a QWP, an HWP, or a PMF segment, affects its input SOP (SOP_{in}) or output SOP (SOP_{out}). By making good use of this WOA finding method, we draw out WOA sets of the four waveplates, which can provide arbitrary phase retardations ϕ's from 0° to 360° to a GTF chosen here arbitrarily. Finally, we show phase-modulated GTF's calculated at eight selected WOA sets allowing ϕ's to be 0°, 45°, 90°, 135°, 180°, 225°, 270°, and 315°, and then the theoretically predicted results are verified by experimentally measured ones. It is concluded from the theoretical and experimental demonstrations that the GTF of our filter based on the OWS of a QWP and an HWP can be arbitrarily phase-modulated, i.e., wavelength-tuned, by properly adjusting the WOA's of the four waveplates.

2. Phase Modulation Principle Based on Spectral Evolution of State of Polarization (SOP)

Figure 1a shows a schematic diagram of the proposed comb filter comprised of a PBS, two PMF segments whose lengths are equal (denoted by PMF 1 and PMF 2), two QWPs (denoted by QWP 1 and QWP 2), and two HWPs (denoted by HWP 1 and HWP 2). As shown in Figure 1a, one OWS of QWP 1 and HWP 1 is placed ahead of PMF 1, and the other OWS of QWP 2 and HWP 2 is located between PMF 1 and PMF 2. Every OWS can effectively change the phase delay difference between two principal modes of the individual PMF segment, and the combination of QWP 2 and HWP 2, or the second OWS, has an additional function to effectively modify the relative angular difference between the principal axes of PMF 1 and PMF 2. The slow axis of PMF 2 butt-coupled to port 3 of the PBS is 22.5° away from the TM polarization axis (denoted by x axis) of the PBS. An input beam introduced into port IN of the filter is decomposed into two orthogonal linear polarization components, such as linear horizontal polarization (LHP) and linear vertical polarization (LVP), which circulate through the polarization-diversified loop of the filter in the clockwise (CW) and counterclockwise (CCW) directions, respectively. Figure 1b shows the two propagation paths of light travelling through the filter, designated as CW and CCW paths. When the SOP_{in} of the filter is LHP, input light propagates along the CW path and sequentially passes through a linear horizontal polarizer (x axis), QWP 1 (with its slow axis oriented at θ_{Q1} for the x axis), HWP 1 (oriented at θ_{H1}), PMF 1 (oriented at θ_{P1}), QWP 2 (oriented at θ_{Q2}), HWP 2 (oriented at θ_{H2}), PMF 2 (oriented at θ_{P2} = 22.5°), and a linear horizontal analyzer (x axis). In the case of the SOP_{in} of LVP, input light propagates through a linear vertical polarizer (y axis), PMF 2 ($-\theta_{P2}$ oriented), HWP 2 ($-\theta_{H2}$ oriented), QWP 2 ($-\theta_{Q2}$ oriented), PMF 1 ($-\theta_{P1}$ oriented), HWP 1 ($-\theta_{H1}$ oriented), QWP 1 ($-\theta_{Q1}$ oriented), and a linear vertical analyzer (y axis) in turn, circulating along the CCW path. F and S displayed on the waveplates and the PMFs indicate their fast and slow axes, respectively.

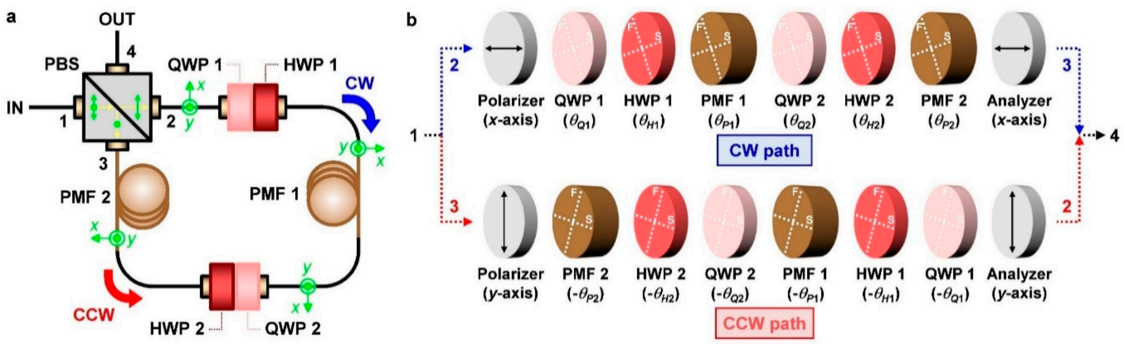

Figure 1. (**a**) Schematic diagram of the PDLS-based first-order fiber comb filter and (**b**) propagation path of light travelling through the filter.

Polarization interference is created by optical birefringence in an optical structure composed of two linear polarizers and BEs inserted between them. In the case of one BE like a PMF segment, the transmittance function of this optical structure becomes a sinusoidally varying function of Γ, the phase delay difference between two principal modes of the BE, which is represented by $2\pi BL/\lambda$, where B, L, and λ are the birefringence of the BE, the length of the BE, and the free space wavelength, respectively. It is possible to tune the wavelength of this polarization interference spectrum by modifying Γ, and the modification of Γ can be done by adding a supplementary phase delay difference ϕ to Γ and modulating this ϕ [21]. In the same way, to tune the wavelength position of the first-order comb spectrum generated with two BEs, or two PMF segments [26], ϕ, which is added to Γ for individual PMF, should be modulated equally for both PMF 1 and PMF 2. This simultaneous ϕ modulation can be accomplished by changing the SOP_{in}'s of PMF 1 and PMF 2 with two OWS's. When we increase ϕ from 0° to 360° by appropriately adjusting the SOP_{in} of each PMF, the comb spectrum makes a redshift by an interference period, i.e., a free spectral range (FSR). The filter transmittance function t_{filter} can be derived from the Jones transfer matrix [27] T given by (1) and is represented as (2). In this derivation, no insertion losses are assumed to exist in any optical components of the filter, and all waveplates are regarded as wavelength-independent.

$$\begin{aligned} T = \begin{bmatrix}1 & 0\\0 & 0\end{bmatrix} T_{PMF2}(\theta_{P2}) T_{HWP2}(\theta_{H2}) T_{QWP2}\big(\theta_{Q2}\big) T_{PMF1}(\theta_{P1}) T_{HWP1}(\theta_{H1}) T_{QWP1}\big(\theta_{Q1}\big) \begin{bmatrix}1 & 0\\0 & 0\end{bmatrix} \\ + \begin{bmatrix}0 & 0\\0 & 1\end{bmatrix} T_{QWP1}\big(-\theta_{Q1}\big) T_{HWP1}(-\theta_{H1}) T_{PMF1}(-\theta_{P1}) \times \\ T_{QWP2}\big(-\theta_{Q2}\big) T_{HWP2}(-\theta_{H2}) T_{PMF2}(-\theta_{P2}) \begin{bmatrix}0 & 0\\0 & 1\end{bmatrix} \end{aligned} \quad (1)$$

$$t_{filter} = \frac{1}{4}(P_0 + P_1\cos\Gamma + P_2\sin\Gamma)^2 + \frac{1}{4}(Q_0 + Q_1\cos\Gamma + Q_2\sin\Gamma)^2 \quad (2)$$

Here, T_{QWP1}, T_{HWP1}, T_{PMF1}, T_{QWP2}, T_{HWP2}, and T_{PMF2} mean the transfer matrices of QWP 1, HWP 1, PMF 1, QWP 2, HWP 2, and PMF 2, whose slow-axis orientation angles are θ_{Q1}, θ_{H1}, θ_{P1}, θ_{Q2}, θ_{H2}, and θ_{P2} (given by 22.5° here) for the x axis, respectively. $P_0 = -\sin\alpha\sin\beta - \sin(\gamma - \pi/4)\sin(\delta - 2\theta_{P1})$, $Q_0 = \cos\gamma\cos\beta - \cos(\alpha - \pi/4)\cos(\delta - 2\theta_{P1})$, $P_1 = -\sin\alpha\sin\beta + \sin(\gamma - \pi/4)\sin(\delta - 2\theta_{P1})$, $Q_1 = \cos\gamma\cos\beta + \cos(\alpha - \pi/4)\cos(\delta - 2\theta_{P1})$, $P_2 = \cos(\gamma - \pi/4)\cos\beta + \cos\alpha\cos(\delta - 2\theta_{P1})$, and $Q_2 = \sin(\alpha - \pi/4)\sin\beta - \sin\gamma\sin(\delta - 2\theta_{P1})$, where $\alpha = 2\theta_{H2} - (\theta_{Q1} + \theta_{Q2})$, $\beta = 2\theta_{H1} - (\theta_{Q1} + \theta_{Q2})$, $\gamma = 2\theta_{H2} + (\theta_{Q1} - \theta_{Q2})$, and $\delta = 2\theta_{H1} - (\theta_{Q1} - \theta_{Q2})$.

Before we begin to address the principle of the phase modulation of a GTF, let us consider the previous conclusions on the relationship between SOP changes and the continuous wavelength tuning of a narrowband transmittance t_n given by (3) in the comb filter composed of two PMF segments, two OWS's of an HWP and a QWP, and the third HWP. [23,24].

$$t_n = [3 - 4\cos(\Gamma + \phi) + \cos 2(\Gamma + \phi)]/8 \quad (3)$$

The additional phase delay difference ϕ in (3) defines the absolute wavelength position of the narrowband transmission spectrum. In the previous studies [23,24], eight WOA sets (from Set $\mathrm{I_n}$ to Set $\mathrm{VIII_n}$) of four waveplates (except for the third HWP) were utilized to display eight wavelength-tuned spectra calculated from t_n with eight ϕ values from 0° to 315° (increment: 45°). When the wavelength of input light increases from λ_0 to $\lambda_0 + \Delta\lambda$, where $\Delta\lambda$ implies the FSR, the $\mathrm{SOP_{in}}$ of PMF 2 at Set $\mathrm{I_n}$ ($\phi = 0°$) spectrally evolves on the Poincare sphere, as shown in Figure 2a. This spectral evolution indicated by pink circles is denoted by SE_{in}. With increasing wavelength, the $\mathrm{SOP_{in}}$ moves along the SE_{in} trace rotating CW around the normal vector $\boldsymbol{p_1}$, when $\boldsymbol{p_1}$ points the observer. The rotation direction of the $\mathrm{SOP_{in}}$ can also be thought using a left-hand rule. If the direction of $\boldsymbol{p_1}$ is the same as that of the left thumb, the direction of the rest of the fingers is the rotation direction of the $\mathrm{SOP_{in}}$ with the increase of the wavelength. In general, the $\mathrm{SOP_{out}}$ of the birefringent medium rotates around its slow axis on the Poincare sphere according to the wavelength λ of light passing through the medium. The vector $\boldsymbol{AB}$ connecting A ($2\varepsilon = 0°$, $2\psi = -135°$) and B ($2\varepsilon = 0°$, $2\psi = 45°$), which lie on the Poincare sphere, points the direction of the slow axis of PMF 2 ($\theta_{P2} = 22.5°$) and is denoted by the vector $\boldsymbol{p_2}$. Here, 2ε ($-90° \le 2\varepsilon \le 90°$) and 2ψ ($-180° \le 2\psi \le 180°$) are the latitude and longitude of the Poincare sphere, respectively. For convenience, the plane whose normal vector is $\boldsymbol{p_1}$, that is, the plane of the SE_{in} trace, is designated as the $\mathrm{SOP_{in}}$ plane, and another plane with its normal vector of $\boldsymbol{p_2}$ is designated as the $\mathrm{SOP_{out}}$ plane. Actually, $\boldsymbol{p_2}$ is an axis of revolution, around which the SE_{in} trace moves as ϕ varies. Hence, $\boldsymbol{p_1}$ and the $\mathrm{SOP_{out}}$ plane are parallel, and $\boldsymbol{p_2}$ and the $\mathrm{SOP_{in}}$ plane are parallel, ending up with $\boldsymbol{p_1}$ and $\boldsymbol{p_2}$ being perpendicular. At Set $\mathrm{II_n}$ ($\phi = 45°$), the SE_{in} trace shown in Figure 2a rotates CCW by 45° around both $\boldsymbol{p_1}$ and $\boldsymbol{p_2}$, and thus $\boldsymbol{p_1}$ shown in Figure 2a rotates 45° CCW about $\boldsymbol{p_2}$ as well. Analogously, for the remaining six sets ($\mathrm{III_n}$–$\mathrm{VIII_n}$), the SE_{in} trace at Set $\mathrm{I_n}$ rotates CCW by 90°–315° (with an increment of 45°) around both $\boldsymbol{p_1}$ and $\boldsymbol{p_2}$.

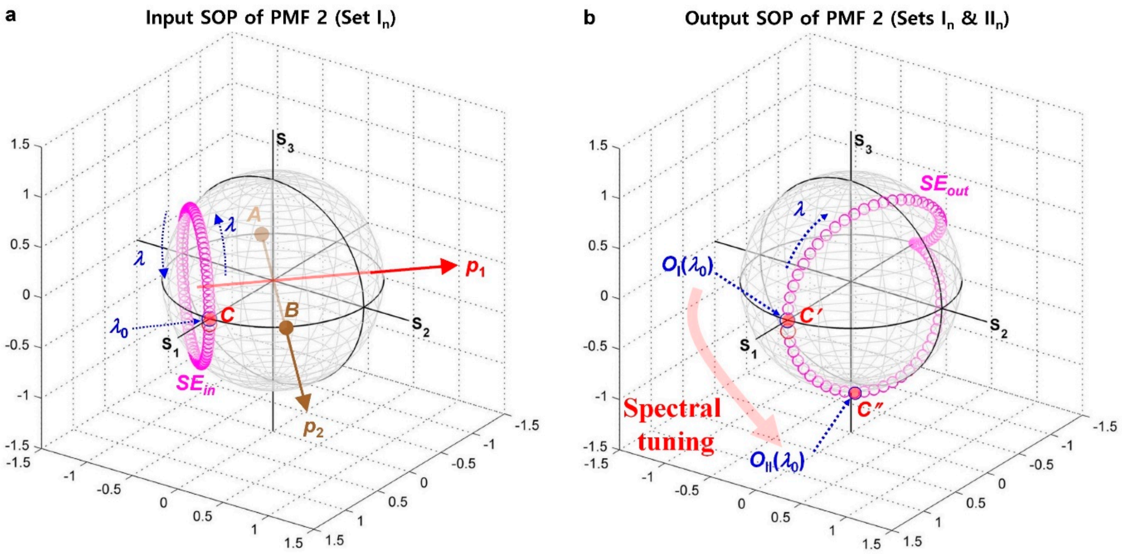

Figure 2. (**a**) Poincare sphere representation of the spectral evolution of SOP_{in} of PMF 2 at Set I_n ($\phi = 0°$), which is denoted by SE_{in} (indicated by pink circles) and (**b**) Poincare sphere representation of the spectral evolution of SOP_{out} of PMF 2, which is denoted by SE_{out} (indicated by pink circles), and two $O(\lambda_0)$ positions at two chosen WOA sets (Sets I_n and II_n). All the SOP traces are obtained in the CW path of Figure 1b over a wavelength range from λ_0 to $\lambda_0 + \Delta\lambda$.

Likewise, the SOP_{out}'s of PMF 2 at Sets I_n ($\phi = 0°$) and II_n ($\phi = 45°$) spectrally evolve on the Poincare sphere over the same wavelength range of λ_0 to $\lambda_0 + \Delta\lambda$, as shown in Figure 2b. This spectral evolution also indicated by pink circles is designated as SE_{out}. This SE_{out} trace is embodied by making a CW rotation of the wavelength-dependent SOP_{in} of PMF 2 about $\boldsymbol{p_2}$ by an angle $\varphi(\lambda)$ given by $360°(\lambda - \lambda_0)/\Delta\lambda$. When PMF 2 is passed through by light at λ_0, the SOP_{in} of PMF 2 at λ_0, C ($2\varepsilon = 0°$, $2\psi = 0°$) shown in Figure 2a, rotates CW around $\boldsymbol{p_2}$ by $\varphi(\lambda_0) = 0°$, and the SOP_{out} of PMF 2 at λ_0 becomes C' ($2\varepsilon = 0°$, $2\psi = 0°$) shown in Figure 2b without a change in the position on the Poincare sphere. Similarly, the SOP_{in} of PMF 2 at $\lambda_0 + \Delta\lambda/4$ rotates CW around $\boldsymbol{p_2}$ by $\varphi(\lambda_0 + \Delta\lambda/4) = 90°$ during its passage through PMF 2. If we put the SOP_{out} of PMF 2 at a certain wavelength λ as $O(\lambda)$, $O(\lambda_0)$ at Set I_n, marked by $O_I(\lambda_0)$ in the figure, becomes C'. Owing to the wavelength-dependent transformation of the SOP_{in} of PMF 2, $O(\lambda)$ forms a non-circular trajectory SE_{out} shaped like a droplet as λ increases from λ_0 to $\lambda_0 + \Delta\lambda$. During the wavelength increase of $\Delta\lambda$ starting from λ_0, $O(\lambda)$ goes round this entire SE_{out} trace starting from C' in the CW direction around the S_2 axis. If we assume the wavelength at which t_n is maximized as λ_{peak}, λ_{peak} can be regarded as λ_0 at Set I_n because t_n reaches the maximum when $O(\lambda)$ is nearest to LHP ($2\varepsilon = 0°$, $2\psi = 0°$) on the Poincare sphere. At Set II_n, $O_{II}(\lambda_0)$, i.e., the SOP_{out} of PMF 2 at λ_0, becomes C'' distant from $O_I(\lambda_0)$ by an angular displacement that corresponds to $\Delta\lambda/8$ and also goes round the entire SE_{out} trace starting from C'' about the S_2 axis in the CW direction, as the wavelength increases from λ_0 to $\lambda_0 + \Delta\lambda$. Here, $O_I(\lambda_0)$ or $O_{II}(\lambda_0)$ is the initial point of the spectral evolution of $O(\lambda)$. The position difference between $O_I(\lambda_0)$ and $O_{II}(\lambda_0)$ originates from the fact that, while the WOA set goes from Set I_n to Set II_n, the SE_{in} trace at Set I_n is rotated CCW by 45° not only about $\boldsymbol{p_1}$ on the SOP_{in} plane but also about $\boldsymbol{p_2}$ on the SOP_{out} plane. This means that simultaneously rotating the SE_{in} trace CCW about both $\boldsymbol{p_1}$ and $\boldsymbol{p_2}$ can change the position of $O(\lambda_0)$ along the SE_{out} trace. On the SE_{out} trace at Set II_n, therefore, $O_{II}(\lambda_0 + \Delta\lambda/8)$ is located at C', and $\lambda_0 + \Delta\lambda/8$ becomes λ_{peak} because C' is nearest to LHP. This implies that the narrowband transmission spectrum moves towards a longer wavelength region by $\Delta\lambda/8$, that is, ϕ is modulated by 45° making t_n be redshifted by $(45°/360°)\Delta\lambda = \Delta\lambda/8$. Similarly, for remaining Sets III_n–$VIII_n$, ϕ is modulated by 90° to 315° with an increment of 45° making t_n be redshifted by $\Delta\lambda/4$ to $7\Delta\lambda/8$ with a step of $\Delta\lambda/8$, and λ_{peak} changes from $\lambda_0 + \Delta\lambda/4$ to $\lambda_0 + 7\Delta\lambda/8$ with an increment of $\Delta\lambda/8$.

In the case of a GTF, or an arbitrary transmittance function, obtained in the proposed filter structure, the SOP_{out} trace of PMF 2, designated as $SE_{out,GTF}$ trace, is presumed to be a completely different trajectory in comparison with the SE_{out} trace shown in Figure 2b. However, it can be deduced from the aforementioned conclusions of the previous works that a location change of $O(\lambda_0)$ along the $SE_{out,GTF}$ trace, accompanied by a shift in λ_{peak}, is responsible for a phase modulation in the GTF, resulting in a wavelength shift in the transmission spectrum. For a given $SE_{out,GTF}$ trace, the corresponding SOP_{in} trace of PMF 2, designated as $SE_{in,GTF}$ trace, should be a circle on the Poincare sphere as well, since a wavelength-dependent BE through which light has passed is just one, PMF 1. However, in terms of the radius and the normal vector ($\boldsymbol{p_1}$) of the circular trace, this $SE_{in,GTF}$ trace will be quite different from the SE_{in} trace shown in Figure 2a. Because it is assumed that all waveplates used here are independent of wavelength, they do not distort the shape of the SOP_{in} or the SOP_{out} trace. Thus, the SOP_{out} trace of PMF 1 also has a circular shape identical to that of the $SE_{in,GTF}$ trace. Like the relationship between the SE_{in} and SE_{out} traces, the increase in λ_{peak} results from the CCW revolution of the $SE_{in,GTF}$ trace about both $\boldsymbol{p_1}$ on the SOP_{in} plane and $\boldsymbol{p_2}$on the SOP_{out} plane. If the $SE_{in,GTF}$ trace is revolved CCW about both $\boldsymbol{p_1}$ and $\boldsymbol{p_2}$ by an amount of ξ, the transmission spectrum makes a redshift of $(\xi/360°)\Delta\lambda$, resulting in an increase of $(\xi/360°)\Delta\lambda$ in λ_{peak}. That is to say, ξ can be regarded as ϕ, or the additional phase delay difference. Thus, as ξ varies from 0° to 360°, the phase of the GTF also changes from 0° to 360°, which means that the GTF is able to be phase-modulated continuously by varying ξ. Briefly, one simultaneous CCW rotation of the $SE_{in,GTF}$ trace about both $\boldsymbol{p_1}$ and $\boldsymbol{p_2}$, implemented by controlling four waveplates contained within the proposed filter, enables its transmission spectrum to be redshifted by an FSR ($\Delta\lambda$), in other words, its phase to be modulated by 360°.

3. Finding Algorithm of Waveplate Orientation Angles (WOA's) for Phase Modulation of General Transmittance Function (GTF)

Considering the aforementioned polarization conditions required for arbitrarily modulating the phase of a GTF or continuously tuning its wavelength, the WOA's (θ_{Q1}, θ_{H1}, θ_{Q2}, θ_{H2}) for this arbitrary phase modulation (i.e., continuous wavelength tuning) are investigated with our unique WOA-finding algorithm. This algorithm is suggested as it is quite sophisticated to draw out an exact mathematical expression of a GTF having an application-specific unique spectrum. Moreover, although the mathematical expression t_{GTF} of a GTF is given, it is cumbersome to solve (θ_{Q1}, θ_{H1}, θ_{Q2}, θ_{H2}) from trigonometric simultaneous equations obtained from direct comparison of t_{GTF} with t_{filter} in (2). To explain our angle-finding approach, let us choose a specific GTF t_{GTF1}, which is procured at a certain selected WOA set (θ_{Q1}, θ_{H1}, θ_{Q2}, θ_{H2}) = (118.23°, 149.56°, 179.42°, 123.46°), and find (θ_{Q1}, θ_{H1}, θ_{Q2}, θ_{H2}) where t_{GTF1} is wavelength-tuned. At the above selected WOA set indicated by Set I_{GTF1} and fixed orientation angles of PMF 1 and PMF 2 (θ_{P1} = 0° and θ_{P2} = 22.5°), the SOP_{out} trace of PMF 2, or $SE_{out,GTF1}$, is obtained over a wavelength range from λ_0 (=1548.0 nm) to $\lambda_0 + \Delta\lambda$ (=0.8 nm), as shown in Figure 3a. At Set I_{GTF1}, $O(\lambda_0)$ indicated in Figure 3a is located nearest to LHP on the Poincare sphere, which makes the filter transmittance be maximized at λ_0. If we put the wavelength at which t_{GTF1} is maximized as λ_{peak}, $O(\lambda_0)$ becomes $O(\lambda_{peak})$, that is, $\lambda_{peak} = \lambda_0$ = 1548.0 nm at Set I_{GTF1}. The SOP_{in} trace of PMF 2, or $SE_{in,GTF1}$ in Figure 3b, can be derived by utilizing the inverse matrix of T_{PMF2} (${T_{PMF2}}^{-1}$) and the $SE_{out,GTF1}$ trace in Figure 3a. Based on the foregoing description on the phase modulation of the GTF using the $SE_{in,GTF}$ and $SE_{out,GTF}$ traces, another $SE_{in,GTF1}$ trace shown in Figure 3c can be obtained by rotating the $SE_{in,GTF1}$ trace at Set I_{GTF1} CCW by 45° around both $\boldsymbol{p_1}$ and $\boldsymbol{p_2}$, for the phase modulation of 45° (i.e., the wavelength tuning of $\Delta\lambda/8$ = 0.1 nm) in t_{GTF1}. It is easily expected that this new $SE_{in,GTF1}$ trace will be obtained at another WOA set (θ_{Q1}, θ_{H1}, θ_{Q2}, θ_{H2}) designated later as Set II_{GTF1}.

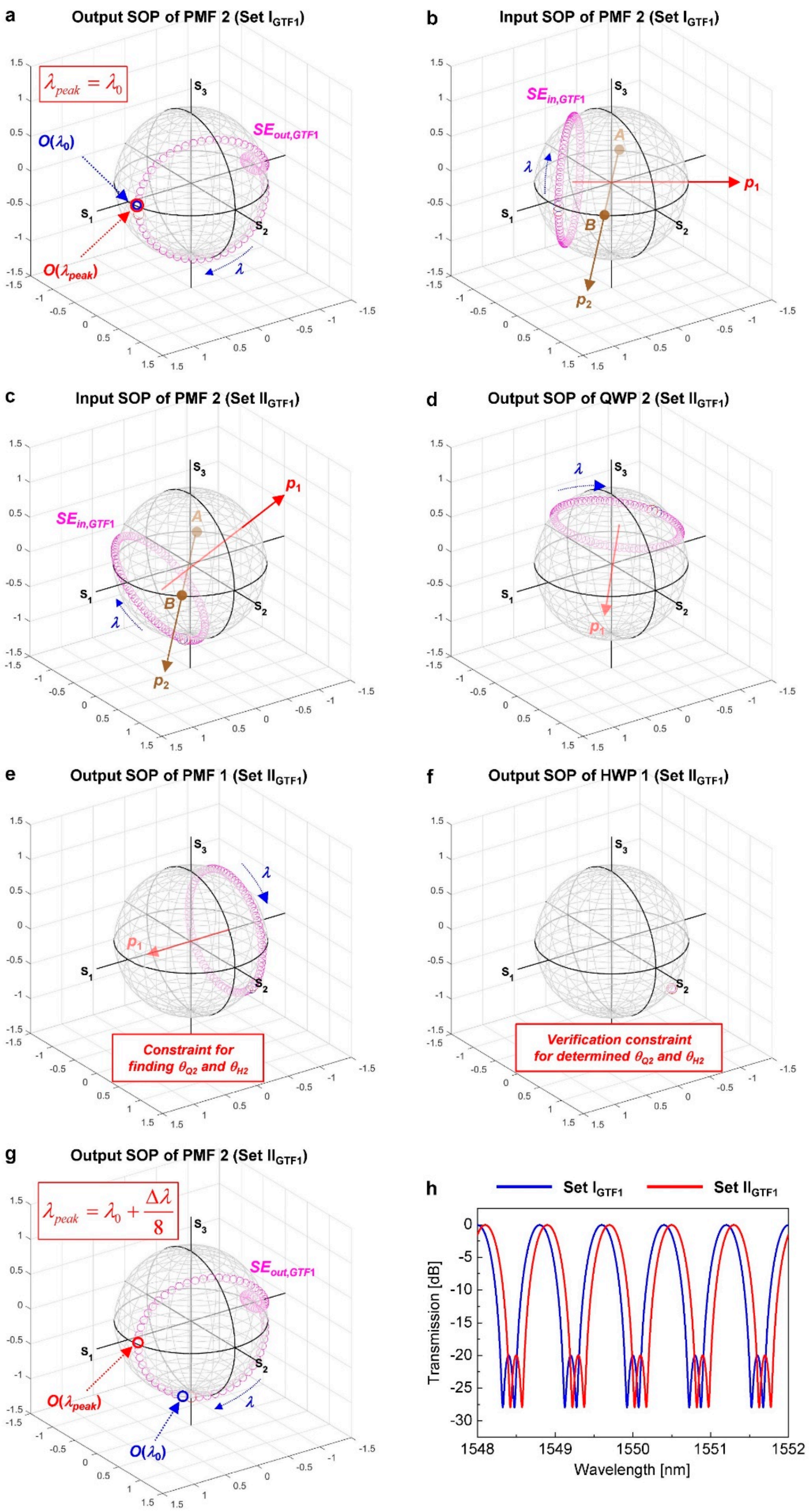

Figure 3. Wavelength-dependent variation of SOP's in t_{GTF1} obtained at Set I_{GTF1}: (**a**) SOP_{out} and (**b**) SOP_{in} traces of PMF 2 at Set I_{GTF1}. Spectral evolution of SOP's in the phase-modulated version of t_{GTF1}, obtained at Set II_{GTF1}: (**c**) SOP_{in} trace of PMF 2, (**d**) SOP_{out} trace of QWP 2, (**e**) SOP_{out} trace of PMF 1, (**f**) SOP_{out} of HWP 1, and (**g**) SOP_{out} trace of PMF 2. (**h**) Two calculated transmission spectra obtained at Sets I_{GTF1} and II_{GTF1}, indicated as blue and red solid lines, respectively.

What we should focus on is a way to obtain Set $\mathrm{II_{GTF1}}$, another WOA set described above. Basically, the $\mathrm{SOP_{out}}$ of one component of the filter is equivalent to the $\mathrm{SOP_{in}}$ of the following component in any propagation path shown in Figure 1b. As our discussion is confined to the CW path, as an example, the $\mathrm{SOP_{out}}$ of PMF 1 is equivalent to the $\mathrm{SOP_{in}}$ of QWP 2. The same thing can be said for SOP traces. For example, the $\mathrm{SOP_{in}}$ trace of HWP 1 is the same as the $\mathrm{SOP_{out}}$ trace of QWP 1. A QWP and an HWP rotate input polarization CCW by 90° and 180° about their slow axes on the Poincare sphere, respectively. If an SOP trace, composed of multiple different SOP's distributed on the Poincare sphere, enters a waveplate, therefore, not its shape but its position is altered by the waveplate. For a given $SE_{in,GTF1}$ trace at Set $\mathrm{II_{GTF1}}$ (in Figure 3c), a certain $\mathrm{SOP_{out}}$ trace of QWP 2 can be obtained by using the $SE_{in,GTF1}$ trace (i.e., the $\mathrm{SOP_{out}}$ trace of HWP 2) and the inverse matrix of T_{HWP2}, or ${T_{HWP2}}^{-1}$, if θ_{H2} is fixed as one value (unknown yet). With this $\mathrm{SOP_{out}}$ trace of QWP 2, shown in Figure 3d, a corresponding $\mathrm{SOP_{out}}$ trace of PMF 1, which is transformed into the $\mathrm{SOP_{out}}$ trace of QWP 2 after passing through QWP 2, can also be derived similarly by using the predetermined $\mathrm{SOP_{out}}$ trace of QWP 2 and ${T_{QWP2}}^{-1}$, if θ_{Q2} is fixed as another value (unknown either), as shown in Figure 3e. Because the SOP rotation due to a QWP or an HWP applies equally to all points comprising an SOP trace, the shape of the SOP trace created by PMF 1 remains the same after passage through HWP 2 or QWP 2, and thus the trajectory shape of the $\mathrm{SOP_{out}}$ trace of QWP 2 or PMF 1 is equal to that of the $SE_{in,GTF1}$ trace. In terms of the $\mathrm{SOP_{out}}$ trace of PMF 1, however, $\boldsymbol{p_1}$, the normal vector of the trace, coincides with the S_1 axis on the Poincare sphere as the orientation angle θ_{P1} of PMF 1 is 0°, as shown in Figure 3e. Then, θ_{H2} and θ_{Q2} can be determined by finding the $\mathrm{SOP_{out}}$ trace of PMF 1 to satisfy this constraint for $\boldsymbol{p_1}$.

After both θ_{H2} and θ_{Q2} are elucidated, the $\mathrm{SOP_{out}}$ of HWP 1, which is displayed as an SOP location on the Poincare sphere, can simply be determined using the $\mathrm{SOP_{out}}$ trace of PMF 1 and ${T_{PMF1}}^{-1}$, as shown in Figure 3f. In particular, the validity of θ_{H2} and θ_{Q2} determined above can be verified by checking whether this $\mathrm{SOP_{in}}$ of PMF 1 is a single SOP point or not. That is to say, if θ_{H2} and θ_{Q2} predetermined abiding by the above constraint for $\boldsymbol{p_1}$ are suitable for the WOA set at Set $\mathrm{II_{GTF1}}$, the $\mathrm{SOP_{in}}$ of PMF 1 should be unchanged even with variations in the wavelength from λ_0 to $\lambda_0 + \Delta\lambda$. As θ_{H2} and θ_{Q2} are found from the $SE_{in,GTF1}$ trace at Set $\mathrm{II_{GTF1}}$, this $\mathrm{SOP_{in}}$ of PMF 1 (i.e., the $\mathrm{SOP_{out}}$ of HWP 1) is the starting point to unveil θ_{H1} and θ_{Q1}. By using the $\mathrm{SOP_{out}}$ of HWP 1 (in Figure 3f) and ${T_{HWP1}}^{-1}$, the $\mathrm{SOP_{out}}$ of QWP 1 can be obtained, if we set θ_{H1} as a fixed value (unknown yet). Moreover, for a fixed value (unknown either) of θ_{Q1}, a corresponding $\mathrm{SOP_{in}}$ of QWP 1 can be drawn out from the above $\mathrm{SOP_{out}}$ of QWP 1 and ${T_{QWP1}}^{-1}$. Then, to find θ_{H1} andθ_{Q1}, we can harness the fundamental SOP constraint that the $\mathrm{SOP_{in}}$ of QWP 1 should be LHP because light emerging from port 2 of the PBS is linear horizontally polarized. Through this reverse tracing algorithm described above, (θ_{Q1}, θ_{H1}, θ_{Q2}, θ_{H2}) at Set $\mathrm{II_{GTF1}}$ could be found to be (108.49°, 132.67°, 201.92°, 134.71°), and it was also confirmed from additional calculations, although not suggested here, that several degenerate WOA sets could also exist for t_{GTF1} at Set $\mathrm{II_{GTF1}}$. It is figured out from the $\mathrm{SOP_{out}}$ trace of PMF 2 at Set $\mathrm{II_{GTF1}}$, the $SE_{out,GTF1}$ trace in Figure 3g, that $O(\lambda_0)$ at Set $\mathrm{II_{GTF1}}$ differs from $O(\lambda_0)$ at Set $\mathrm{I_{GTF1}}$, although the shape of the $SE_{out,GTF1}$ trace at Set $\mathrm{II_{GTF1}}$ remains unchanged in comparison with the shape of the $SE_{out,GTF1}$ trace at Set $\mathrm{I_{GTF1}}$. From $O(\lambda_0)$ at Set $\mathrm{I_{GTF1}}$, $O(\lambda_0)$ at Set $\mathrm{II_{GTF1}}$ is distant by an angular displacement that corresponds to $\Delta\lambda/8$ along this $SE_{out,GTF1}$ trace towards decreasing wavelength. This implies that $O(\lambda_0 + \Delta\lambda/8)$ at Set $\mathrm{II_{GTF1}}$ is the same as $O(\lambda_0)$ at Set $\mathrm{I_{GTF1}}$ and also as $O(\lambda_{peak})$ at Set $\mathrm{II_{GTF1}}$, and λ_{peak} becomes $\lambda_0 + \Delta\lambda/8$ at Set $\mathrm{II_{GTF1}}$, resulting in a wavelength shift of $\Delta\lambda/8$ in t_{GTF1} (i.e., a phase modulation of 45°). Figure 3h shows two transmission spectra of t_{GTF1}, which are calculated at Sets $\mathrm{I_{GTF1}}$ and $\mathrm{II_{GTF1}}$ and displayed by blue and red solid lines, respectively. It is apparent that the transmission spectrum at Set $\mathrm{II_{GTF1}}$ is redshifted by $\Delta\lambda/8$ (= 0.1 nm) compared with that at Set $\mathrm{I_{GTF1}}$. In short, for a phase modulation of η, or a wavelength tuning of $(\eta/360°)\Delta\lambda$, in t_{GTF1}, one should find a new $SE_{in,GTF1}$ trace first, obtained by revolving the $SE_{in,GTF1}$ trace at Set $\mathrm{I_{GTF1}}$ CCW by η in angle about $\boldsymbol{p_1}$ and $\boldsymbol{p_2}$. Then, one can find (θ_{Q1}, θ_{H1}, θ_{Q2}, θ_{H2}) for this new $SE_{in,GTF1}$ trace through the WOA-searching procedures addressed above. If we pick η within 0° to 360°, t_{GTF1} can be arbitrarily phase-modulated. This arbitrary phase modulation can be utilized directly for the continuous wavelength tuning of t_{GTF1}.

4. WOA's for Phase Modulation of GTF and Its Phase-Modulated Spectra

Here, we explore WOA sets for continuous phase modulation of another GTF t_{GTF2}, which is defined at another different (θ_{Q1}, θ_{H1}, θ_{Q2}, θ_{H2}) = (105°, 154°, 17°, 2°) with θ_{P1} = 0° and θ_{P2} = 22.5°, by using our reverse tracing method. Specifically, 360 sets of (θ_{Q1}, θ_{H1}, θ_{Q2}, θ_{H2}), where an additional phase shift of 1°–360° (increment: 1°) can be induced in t_{GTF2}, were found with our method. Figure 4a shows the 360 sets of (θ_{Q1}, θ_{H1}, θ_{Q2}, θ_{H2}) as functions of ϕ ranging from 0° to 360° (step: 1°), displayed by blue circles (θ_{Q1}), green squares (θ_{H1}), red diamonds (θ_{Q2}), and violet triangles (θ_{H2}), respectively, which are found at fixed values of θ_{P1} = 0° and θ_{P2} = 22.5°. In contrast with WOA sets for continuous wavelength tuning of an analytic transmittance t_n [23,24], all four WOA's (θ_{Q1}, θ_{H1}, θ_{Q2}, and θ_{H2}) do not take the form of simple mathematical functions of ϕ and have similar patterns either. Whereas $\theta_{Q1}(\phi)$ and $\theta_{H1}(\phi)$ have a period of 180°, the period of $\theta_{Q2}(\phi)$ or $\theta_{H2}(\phi)$ is 360°. θ_{Q1}, θ_{H1}, θ_{Q2}, and θ_{H2} are bounded in the WOA ranges of 63.5° < θ_{Q1} < 116.6°, 115.4° < θ_{H1} < 154.6°, −37.2° < θ_{Q2} < 37.2°, and −18.1° < θ_{H2} < 40.6°, respectively. In order to reveal implicit information on the 360 sets of (θ_{Q1}, θ_{H1}, θ_{Q2}, θ_{H2}) in Figure 4a, we investigated the relationship between any two of the four WOA's. Figure 4b shows the loci of (θ_{H2}, θ_{H1}) and (θ_{H2}, θ_{Q1}), displayed by blueish squares and reddish circles, respectively. These loci were drawn using $\theta_{H2}(\phi)$, $\theta_{H1}(\phi)$, and $\theta_{Q1}(\phi)$ in Figure 4a in the Cartesian coordinate system at a range of ϕ from 0° to 360°. As ϕ increases from 0° to 360°, (θ_{H2}, θ_{H1}) or (θ_{H2}, θ_{Q1}) forms a closed locus, whose shape is similar to a squeezed goggle or an infinity symbol, respectively. Because the period of $\theta_{H2}(\phi)$ is two times longer than that of $\theta_{H1}(\phi)$ or $\theta_{Q1}(\phi)$, both loci have two-fold symmetry. It is readily seen that the density of the point (θ_{H2}, θ_{H1}) or (θ_{H2}, θ_{Q1}), the interval between two locus points, is different along the locus. In terms of the locus of (θ_{H2}, θ_{H1}), the lower inner part of the locus is sparser than its other parts. This implies that the ϕ variation is smaller at the lower inner part of the locus for the same amounts of changes in θ_{H2} and θ_{H1}. Similarly, in terms of the locus of (θ_{H2}, θ_{Q1}), the upper part of the locus is denser than its lower part, which means that the ϕ variation is larger at the upper part of the locus for the same amounts of changes in θ_{H2} and θ_{Q1}. Next, the loci of (θ_{Q1}, θ_{H1}) and (θ_{Q1}, θ_{Q2}), displayed by blueish squares and reddish circles, are plotted with $\theta_{Q1}(\phi)$, $\theta_{H1}(\phi)$, and $\theta_{Q2}(\phi)$ in Figure 4a at ϕ ranges of 0°–180° and 0°–360°, respectively, as shown in Figure 4c. In terms of the locus of (θ_{Q1}, θ_{H1}), the point of (θ_{Q1}, θ_{H1}) makes a round along this elliptical locus from (105°, 154°) in the CW direction, while ϕ increases from 0° to 180°. It can be seen that the right side of this elliptical locus is much denser than its left side, which suggests that an equal displacement of the point (θ_{Q1}, θ_{H1}) on the locus results in a relatively greater change in ϕ at the right side. Even if the (θ_{Q1}, θ_{H1}) locus is not represented using analytic mathematical expressions as suggested in the previous work [22], the desirable phase ϕ, i.e., the desirable transmission dip (or peak) wavelength, can be set and be continuously changed by selecting and shifting (θ_{Q1}, θ_{H1}) on this locus, respectively, while letting θ_{Q2} and θ_{H2} follow the WOA curves of $\theta_{Q2}(\phi)$ and $\theta_{H2}(\phi)$ in Figure 4a, respectively. In terms of the locus of (θ_{Q1}, θ_{Q2}), the point of (θ_{Q1}, θ_{Q2}) makes a closed parabolic trace for ϕ increasing from 0° to 360°. Like the (θ_{H2}, θ_{H1}) and (θ_{H2}, θ_{Q1}) loci in Figure 4b, this (θ_{Q1}, θ_{Q2}) locus also has a two-fold symmetry with respect to the θ_{Q1} axis because $\theta_{Q2}(\phi)$ has a period two times longer than $\theta_{Q1}(\phi)$. Moreover, the density difference on the locus is analogous to that of the (θ_{Q1}, θ_{H1}) locus. Figure 4d shows the loci of (θ_{Q2}, θ_{H1}) and (θ_{Q2}, θ_{H2}), displayed by blueish squares and reddish circles, respectively. $\theta_{Q2}(\phi)$, $\theta_{H1}(\phi)$, and $\theta_{H2}(\phi)$ in Figure 4a are utilized to plot these loci at a ϕ range of 0°–360°. (θ_{Q2}, θ_{H1}) forms a locus shaped like inverted Spiderman's eyes with increasing ϕ (from 0° to 360°), which also has a two-fold symmetry with respect to the θ_{H1} axis owing to the period of $\theta_{Q2}(\phi)$ two times longer than that of $\theta_{H1}(\phi)$. It can also be found that the lower outer part of the (θ_{Q2}, θ_{H1}) locus is sparser than its other parts. The locus of (θ_{Q2}, θ_{H2}) forms a parallelogram-shaped trace, which makes one CW revolution along the locus, starting at (17°, 2°), while ϕ varies from 0° to 360°. The left and right sides of the (θ_{Q2}, θ_{H2}) locus are slightly sparser than its other parts. This indicates that an identical displacement of the point (θ_{Q2}, θ_{H2}) along the locus causes a relatively smaller modification of ϕ at these parts of the locus. In sum, it is confirmed from Figure 4 that one can always find a WOA set (θ_{Q1}, θ_{H1}, θ_{Q2}, θ_{H2}) with respect to any ϕ (increasing from 0° to 360° by 1°). This means that the phase of t_{GTF2} can be continuously modulated, also indicating that t_{GTF2} can be continuously frequency-tuned. As long as an initial WOA set where any GTF is obtained is given, one can always find a WOA set inducing an arbitrary phase in this GTF.

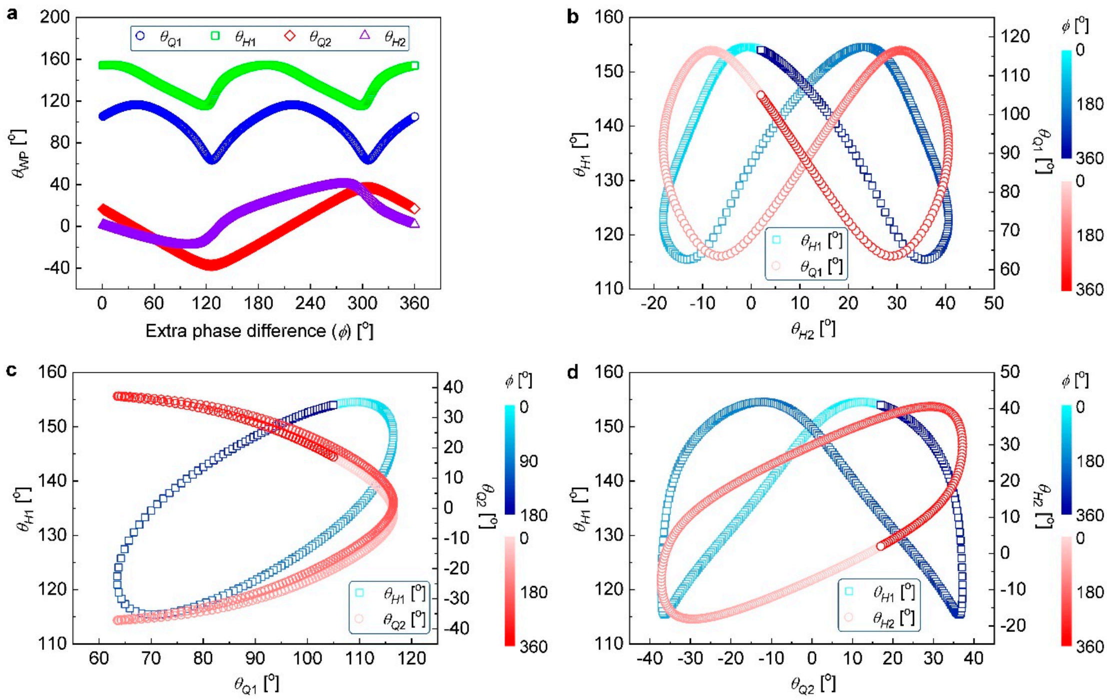

Figure 4. (**a**) Four WOA's θ_{Q1} (blue circles), θ_{H1} (green squares), θ_{Q2} (red diamonds), and θ_{H2} (violet triangles) as a function of extra phase difference ϕ (from 0° to 360° with a step of 1°) for phase modulation of another GTF (t_{GTF2}) at θ_{P1} = 0° and θ_{P2} = 22.5°. (**b**) Loci of (θ_{H2}, θ_{H1}) and (θ_{H2}, θ_{Q1}), displayed by blueish squares and reddish circles, respectively. (**c**) Loci of (θ_{Q1}, θ_{H1}) and (θ_{Q1}, θ_{Q2}), indicated as blueish squares (ϕ: 0°–180°) and reddish circles (ϕ: 0°–360°), respectively. (**d**) Loci of (θ_{Q2}, θ_{H1}) and (θ_{Q2}, θ_{H2}), displayed by blueish squares and reddish circles, respectively.

To examine if the WOA sets found by our angle-finding method can embody the predicted continuous phase modulation of t_{GTF2}, the transmission spectra of t_{GTF2} were calculated at eight WOA sets, which were chosen from the WOA sets found above for the phase modulation of t_{GTF2}, with θ_{P1} and θ_{P2} set at 0° and 22.5°, respectively. The chosen WOA sets, denoted by Sets $\mathrm{I_{GTF2}}$, $\mathrm{II_{GTF2}}$, $\mathrm{III_{GTF2}}$, $\mathrm{IV_{GTF2}}$, $\mathrm{V_{GTF2}}$, $\mathrm{VI_{GTF2}}$, $\mathrm{VII_{GTF2}}$, and $\mathrm{VIII_{GTF2}}$, enable ϕ's to be chosen as 0°, 45°, 90°, 135°, 180°, 225°, 270°, and 315°, respectively. The transmission spectra of the GTF t_{GTF2}, shown in Figure 5, were calculated at the eight WOA sets (Sets $\mathrm{I_{GTF2}}$–$\mathrm{VIII_{GTF2}}$) in a wavelength range of 1548–1552 nm. For the calculation of the transmission spectrum, the length L and birefringence B of PMF (PMF 1 or PMF 2) were set as 7.2 m and 4.166 × 10^{-4}, respectively, so that $\Delta\lambda$ became ~0.8 nm at 1550 nm. It can be seen from the figure that the first-order comb spectrum of deformed narrow passbands makes a redshift as ϕ is modulated as 0° to 315° (increment: 45°). If the peak wavelength of one passband is designated as $\lambda_{peak,GTF}$ at Set $\mathrm{I_{GTF2}}$ (ϕ = 0°), one step transition in the WOA set (e.g., from Set $\mathrm{II_{GTF2}}$ to Set $\mathrm{III_{GTF2}}$) leads to an increase of 45° in ϕ and of 0.1 nm in $\lambda_{peak,GTF}$. Linear movement of $\lambda_{peak,GTF}$ with respect to ϕ, displayed as red-dotted arrows, directly tells us that the continuous or the desired arbitrary phase modulation of t_{GTF2} can be realized. These calculation results clearly manifest that t_{GTF2} can be continuously wavelength-shifted within $\Delta\lambda$ using the WOA sets shown in Figure 4, implying the arbitrary phase modulation capability of t_{GTF2} within 360°.

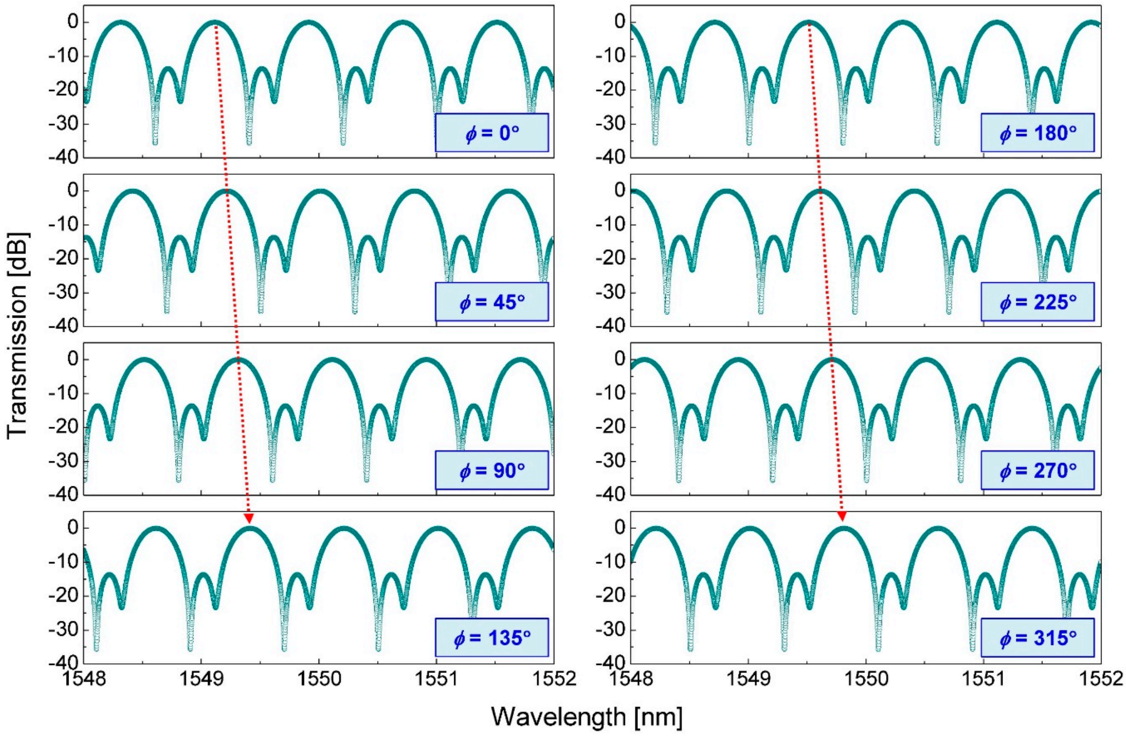

Figure 5. Calculated phase-modulated transmission spectra of GTF (t_{GTF2}), obtained at eight WOA sets (Sets $\mathrm{I_{GTF2}}$–$\mathrm{VIII_{GTF2}}$) where ϕ of t_{GTF2} is chosen as 0° to 315° with an increment of 45°.

5. Experimental Verification of Phase-Modulated Spectra

In order to verify the predicted phase modulation capability of t_{GTF2} through experiments, our filter was manufactured with a fiber-pigtailed PBS (OZ Optics) with four ports, two fiber-pigtailed QWPs (OZ Optics), two fiber-pigtailed HWPs (OZ Optics), and two ~7.12 m-long segments of bow-tie PMF (Fibercore) with a birefringence of ~4.166×10^{-4}, as shown in Figure 1a. Figure 6 shows an actual experimental setup for measuring the transmission spectrum of the constructed filter. As shown in Figure 6, we employed a broadband light source (BLS, Fiberlabs FL7701) covering S, C, and L bands and an optical spectrum analyzer (OSA, Yokogawa AQ6370C) to monitor the transmission spectra of the constructed filter. The input and output ports (ports 1 and 4) of the filter were connected to the BLS and OSA, respectively, with optical fiber patchcords (FC/PC type). For acquisition of high resolution and contrast optical spectra, we set the sensitivity and resolution bandwidth of the OSA as HIGH1 and 0.05 nm, respectively. To avoid unwanted position changes of all the optical components comprising the filter, we taped them up on the optical table so that they were immobilized during the spectrum measurement.

The transmission spectra of the GTF t_{GTF2}, shown in Figure 7, were measured at the eight WOA sets (Sets $\mathrm{I_{GTF2}}$–$\mathrm{VIII_{GTF2}}$) in a wavelength range of 1548–1552 nm. From the measured spectra, the FSR of the constructed filter was evaluated as ~0.8 nm around 1550 nm. This FSR is determined by L (~7.12 m) and B (~4.166×10^{-4}) of PMF used here and increases with wavelength. As confirmed from the theoretical spectra in Figure 5, while the WOA set is switched from Set $\mathrm{I_{GTF2}}$ (ϕ = 0°) to Set $\mathrm{VIII_{GTF2}}$ (ϕ = 315°), the comb spectrum of deformed narrow passbands, which seems to be analogous to the comb spectrum shown in Figure 5, shifts towards a longer wavelength region step by step by ~0.1 nm, resulting in a total wavelength displacement of ~0.7 nm. The inset shows the variation of $\lambda_{peak,GTF}$ (indicated as a red-dotted arrow) according to eight values of ϕ, i.e., 0°, 45°, 90°, 135°, 180°, 225°, 270°, and 315°, which are obtained at Sets $\mathrm{I_{GTF2}}$, $\mathrm{II_{GTF2}}$, $\mathrm{III_{GTF2}}$, $\mathrm{IV_{GTF2}}$, $\mathrm{V_{GTF2}}$, $\mathrm{VI_{GTF2}}$, $\mathrm{VII_{GTF2}}$, and $\mathrm{VIII_{GTF2}}$, respectively. Blue squares designated as $\mathrm{I_{GTF2}}$–$\mathrm{VIII_{GTF2}}$ indicate the $\lambda_{peak,GTF}$ positions of transmission spectra obtained at eight Sets $\mathrm{I_{GTF2}}$–$\mathrm{VIII_{GTF2}}$. It can be figured out from the inset that

$\lambda_{peak,GTF}$ very linearly increases with ϕ showing an adjusted R^2 value of ~0.99946 and the tuning of the spectrum wavelength can be mediated by the phase modulation. In particular, through additional experiments, continuous frequency tuning capability was confirmed with respect to numerous ϕ values arbitrarily selected from 0° to 360° except integer multiples of 45° as well. Thus, it is experimentally verified that the GTF t_{GTF2} can be arbitrarily phase-modulated by properly controlling (θ_{Q1}, θ_{H1}, θ_{Q2}, θ_{H2}), specifically, appropriately selecting (θ_{Q1}, θ_{H1}, θ_{Q2}, θ_{H2}) that satisfies the WOA sets suggested in Figure 4. Ultimately, we conclude that any GTF generated in the proposed comb filter can be phase-modulated, or wavelength-tuned, continuously by taking advantage of WOA sets that can always be drawn out with our reverse tracing algorithm.

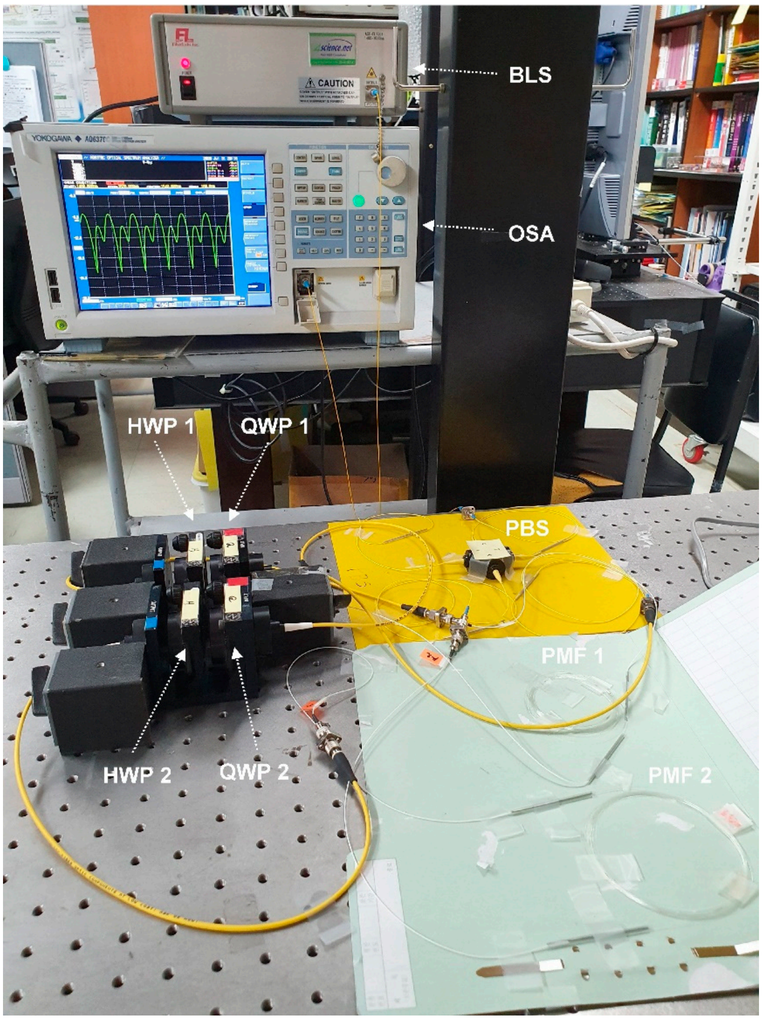

Figure 6. Actual experimental setup for measurement of phase-modulated transmission spectra of GTF (t_{GTF2}).

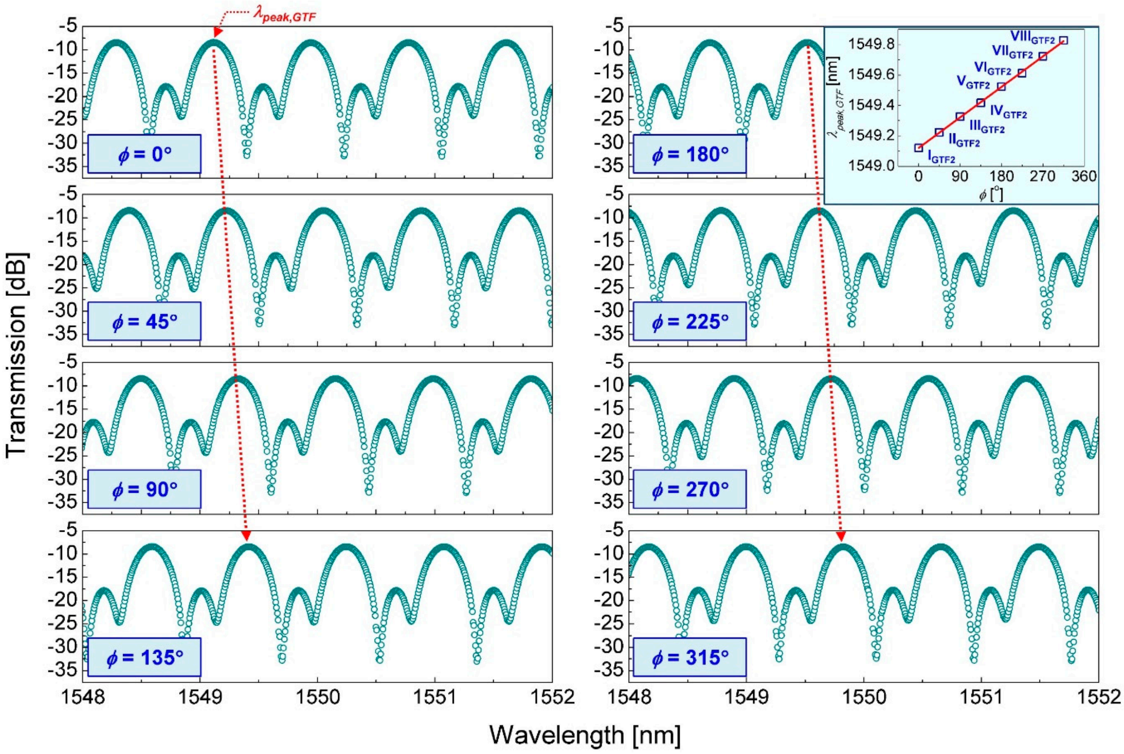

Figure 7. Experimental phase-modulated transmission spectra of GTF (t_{GTF2}), measured at eight WOA sets (Sets $\mathrm{I_{GTF2}}$–$\mathrm{VIII_{GTF2}}$).

6. Conclusions

We demonstrated the arbitrary phase modulation of a GTF, which could be obtained in the first-order fiber comb filter based on the PDLS. The proposed filter was composed of a PBS, two OWS's of an HWP and a QWP, and two PMF segments. Each OWS was located before each PMF segment, and the second PMF segment was butt-coupled to one port of the PBS so that its principal axis should be 22.5° away from the TM polarization axis of the PBS. Basically, polarization conditions, which should be satisfied to modify the phase of a GTF as a desired value, were explained using the spectral evolution of the $\mathrm{SOP_{in}}$ and $\mathrm{SOP_{out}}$ of the second PMF in the narrowband transmittance function (t_n), on the basis of the continuous wavelength tuning mechanism of previously reported PDLS-based first-order narrowband comb filters. Then, we explained a systematic scheme to find four WOA's for the arbitrary phase modulation of a GTF using the effect of each component of the filter, such as a waveplate or PMF segment, on its $\mathrm{SOP_{in}}$ or $\mathrm{SOP_{out}}$. By exploiting this WOA finding method, we derived WOA sets of the four waveplates, which could give arbitrary phase delays ϕ's from 0° to 360° to a GTF chosen here arbitrarily. Finally, we showed phase-modulated GTF's calculated at eight selected WOA sets allowing ϕ's to be 0°, 45°, 90°, 135°, 180°, 225°, 270°, and 315°, and then the theoretically predicted results were experimentally verified. It is concluded from the theoretical and experimental demonstrations that the GTF of our filter based on the OWS of a QWP and an HWP can be arbitrarily phase-modulated by appropriately controlling the WOA's of the four waveplates. Our demonstration is expected to be beneficial to fiber-optic applications, which demand frequency-tunable comb filters with specific transmittances, such as microwave photonic signal processing, optical sensor interrogation, and multiwavelength lasing.

Author Contributions: Conceptualization, J.J. and Y.W.L.; methodology, J.J.; software, J.J.; validation, J.J. and Y.W.L.; formal analysis, Y.W.L.; investigation, Y.W.L.; resources, J.J. and Y.W.L.; data curation, Y.W.L.; writing—original draft preparation, J.J.; writing—review and editing, J.J. and Y.W.L.; visualization, J.J. and Y.W.L.; supervision, Y.W.L.; project administration, Y.W.L.; funding acquisition, Y.W.L. All authors have read and agreed to the published version of the manuscript.

Funding: This research was supported by Basic Science Research Program through the National Research Foundation of Korea (NRF) funded by the Ministry of Education(2019R1I1A3A01046232).

Conflicts of Interest: The authors declare no conflict of interest.

References

1. Li, J.; Xu, K.; Fu, S.; Tang, M.; Shum, P.; Wu, J.; Lin, J. Photonic polarity-switchable ultra-wideband pulse generation using a tunable Sagnac interferometer comb filter. *IEEE Photonics Technol. Lett.* **2008**, *20*, 1320–1322. [CrossRef]
2. Nguimdo, R.M.; Verschaffelt, G.; Danckaert, J.; Van der Sande, G. Fast photonic information processing using semiconductor lasers with delayed optical feedback: Role of phase dynamics. *Opt. Express* **2014**, *22*, 8672–8686. [CrossRef]
3. Lacava, C.; Ettabib, M.; Petropoulos, P. Nonlinear silicon photonic signal processing devices for future optical networks. *Appl. Sci.* **2017**, *7*, 103. [CrossRef]
4. Bian, S.Y.; Ren, M.Q.; Wei, L. A wavelength spacing switchable and tunable high-birefringence fiber loop mirror filter. *Microw. Opt. Technol. Lett.* **2014**, *56*, 1666–1670. [CrossRef]
5. Ge, J.; Fok, M.P. Passband switchable microwave photonic multiband filter. *Sci. Rep.* **2015**, *5*, 15882. [CrossRef]
6. Guo, J.-J.; Yang, Y.; Peng, G.-D. Analysis of polarization-independent tunable optical comb filter by cascading MZI and phase modulating Sagnac loop. *Opt. Commun.* **2011**, *284*, 5144–5147. [CrossRef]
7. Luo, Z.-C.; Cao, W.-J.; Luo, A.-P.; Xu, W.-C. Polarization-independent, multifunctional all-fiber comb filter using variable ratio coupler-based Mach–Zehnder interferometer. *J. Lightwave Technol.* **2012**, *30*, 1857–1862. [CrossRef]
8. Sun, G.; Moon, D.S.; Lin, A.; Han, W.T.; Chung, Y. Tunable multiwavelength fiber laser using a comb filter based on erbium-ytterbium co-doped polarization maintaining fiber loop mirror. *Opt. Express* **2008**, *16*, 3652–3658. [CrossRef]
9. Pottiez, O.; Ibarra-Escamilla, B.; Kuzin, E.A.; Grajales-Coutino, R.; Gonzalez-Garcia, A. Tunable Sagnac comb filter including two wave retarders. *Opt. Laser Technol.* **2010**, *42*, 403–408. [CrossRef]
10. Sova, R.M.; Kim, C.S.; Kang, J.U. Tunable dual-wavelength all-PM fiber ring laser. *IEEE Photonics Technol. Lett.* **2002**, *14*, 287–289. [CrossRef]
11. Luo, Z.-C.; Luo, A.-P.; Xu, W.-C.; Yin, H.-S.; Liu, J.-R.; Ye, Q.; Fang, Z.-J. Tunable multiwavelength passively mode-locked fiber ring laser using intracavity birefringence-induced comb filter. *IEEE Photonics J.* **2010**, *2*, 571–577. [CrossRef]
12. Lee, Y.W.; Han, K.J.; Lee, B.; Jung, J. Polarization-independent all-fiber multiwavelength-switchable filter based on a polarization-diversity loop configuration. *Opt. Express* **2003**, *11*, 3359–3364. [CrossRef]
13. Lee, Y.W.; Han, K.J.; Jung, J.; Lee, B. Polarization-independent tunable fiber comb filter. *IEEE Photonics Technol. Lett.* **2004**, *16*, 2066–2068. [CrossRef]
14. Roh, S.; Chung, S.; Lee, Y.W.; Yoon, I.; Lee, B. Channel-spacing-and wavelength-tunable multiwavelength fiber ring laser using semiconductor optical amplifier. *IEEE Photonics Technol. Lett.* **2006**, *18*, 2302–2304. [CrossRef]
15. Yoon, I.; Lee, Y.W.; Jung, J.; Lee, B. Tunable multiwavelength fiber laser employing a comb filter based on a polarization-diversity loop configuration. *J. Lightwave Technol.* **2006**, *24*, 1805–1811. [CrossRef]
16. Lee, Y.W.; Kim, H.-T.; Jung, J.; Lee, B. Wavelength-switchable flat-top fiber comb filter based on a Solc type birefringence combination. *Opt. Express* **2005**, *13*, 1039–1048. [CrossRef]
17. Lee, Y.W.; Kim, H.-T.; Lee, Y.W. Second-order all-fiber comb filter based on polarization-diversity loop configuration. *Opt. Express* **2008**, *16*, 3871–3876. [CrossRef]
18. Jo, S.; Kim, Y.; Lee, Y.W. Study on transmission and output polarization characteristics of a first-order Lyot-type fiber comb filter using polarization-diversity loop. *IEEE Photonics J.* **2015**, *7*, 1–15. [CrossRef]
19. Park, K.; Lee, Y.W. Zeroth-and first-order-convertible fiber interleaving filter. *IEEE Photonics J.* **2016**, *8*, 1–10. [CrossRef]
20. Park, K.; Choi, S.; Lee, S.-L.; Jeong, J.H.; Jeong, S.J.; Christian, N.J.; Kim, M.S.; Kim, J.; Kang, H.W.; Nam, S.Y.; et al. Second-order fiber interleaving filter based on polarization-diversified loop. *Opt. Eng.* **2017**, *56*, 066108. [CrossRef]

21. Jung, J.; Lee, Y.W. Tunable fiber comb filter based on simple waveplate combination and polarization-diversified loop. *Opt. Laser Technol.* **2017**, *91*, 63–70. [CrossRef]
22. Jung, J.; Lee, Y.W. Continuously wavelength-tunable passband-flattened fiber comb filter based on polarization-diversified loop structure. *Sci. Rep.* **2017**, *7*, 8311. [CrossRef]
23. Jung, J.; Lee, Y.W. Polarization-independent wavelength-tunable first-order fiber comb filter. *IEEE Photonics J.* **2019**, *11*, 1–15. [CrossRef]
24. Kim, D.K.; Kim, J.; Lee, S.-L.; Choi, S.; Kim, M.S.; Lee, Y.W. Tunable narrowband fiber multiwavelength filter based on polarization-diversified loop structure. *J. Nanosci. Nanotechnol.* **2020**, *20*, 344–350. [CrossRef]
25. Jung, J.; Lee, Y.W. Universal wavelength tuning scheme for a first-order optical fiber multiwavelength filter based on a polarization-diversified loop structure. *J. Nanosci. Nanotechnol.* **2020**, *20*, 460–469. [CrossRef]
26. Fang, X.; Ji, H.; Allen, C.T.; Demarest, K.; Pelz, L. A compound high-order polarization-independent birefringence filter using Sagnac interferometers. *IEEE Photonics Technol. Lett.* **1997**, *9*, 458–460. [CrossRef]
27. Jones, R.C. A new calculus for the treatment of optical systems: I. Description and discussion of the calculus. *J. Opt. Soc. Am.* **1941**, *31*, 488–493.